Precise calculation of the two-step process for $K^-d \to \pi\Sigma N$ in the $\Lambda(1405)$ resonance region

K. Miyagawa[1] and J. Haidenbauer[2,3]
[1] *Simulation Science Center, Okayama University of Science, 1-1 Ridai-cho, Okayama 700-0005, Japan*
[2] *Institute for Advanced Simulation, Forschungszentrum Jülich, D-52425 Jülich, Germany*
[3] *Institut für Kernphysik and Jülich Center for Hadron Physics, Forschungszentrum Jülich, D-52425 Jülich, Germany*

The reaction $K^-d \to \pi\Sigma N$ is investigated taking into account single scattering and the two-step process due to $\bar{K}N \to \pi\Sigma$ rescattering. The influence of some common approximations are examined. It is found that the treatment of the kinematics in the Green's function that appears in the loop integral of the rescattering process has a rather strong impact on the resulting lineshape of the $\pi\Sigma$ invariant mass spectrum. Specifically, a calculation with correct kinematics where the three-body unitarity cut due to the nK^-p threshold occurs at the physical value yields a pronounced peak in the invariant mass spectrum at this threshold and, at the same time, suppresses the signal in the region of the $\Lambda(1405)$ resonance. On the other hand, an approximation applied in past calculations shifts that threshold down and, consequently, leads to an accidental and therefore erroneous enhancement of the signal of the $\Lambda(1405)$ in the $\pi\Sigma$ invariant mass spectrum.

PACS numbers: 13.75.Jz, 12.39.Pn
Keywords:

I. INTRODUCTION

The $\Lambda(1405)$, a baryon resonance with $I(J^P) = 0(\frac{1}{2}^-)$, has intrigued theorists already for several decades. The proximity of its nominal mass [1] to the $\bar{K}N$ threshold (at around 1435 MeV) has led to speculations that this resonance is, in fact, a $\bar{K}N$ (quasi) bound state rather than a genuine 3-quark state as soon as it was experimentally identified in the early 1960s. A further and even more peculiar facet was added to this when it was suggested that the $\Lambda(1405)$ could be actually a superposition of two resonance states [2, 3]. This conjecture emerged from model calculations performed within the so-called chiral unitary approach based on coupled channels ($\bar{K}N$, $\pi\Sigma$, ...).

Subsequent investigations conducted within variants of that approach, utilizing the leading-order chiral Lagrangian (Weinberg-Tomozawa term) as interaction potential but also higher-order contributions, supported the existence of two poles in the energy region of the $\Lambda(1405)$ resonance [4–8]. Thereby it was found that typically one of the poles lies very close to the $\bar{K}N$ threshold, i.e. around 1420-1430 MeV, and couples strongly to the $\bar{K}N$ system [3]. The other pole exhibits a much larger variation from model to model, i.e. is usually located around 1340–1400 MeV (though even values around 1470 MeV are reported [8]) and has usually a much larger width. Furthermore, it couples more strongly to the $\pi\Sigma$ system.

Naturally, the prospect of finding two $\Lambda(1405)$ resonances has trigged also an increased interest in performing corresponding experiments. These experiments are guided by the idea that reactions that are dominated by either the $\bar{K}N$ or the $\pi\Sigma$ transition channels should then also provide evidence for the presence of either the one or the other corresponding pole. Specifically, K^- induced reactions should then be dominated by the pole around 1420 MeV and, accordingly, show an enhancement in the distribution at the corresponding invariant mass [3].

In the present work we consider the reaction $K^-d \to \pi\Sigma N$ where the $\Lambda(1405)$ can be excited. Our study is motivated by a corresponding proposal submitted to the J-PARC 50-GeV proton synchrotron. This proposal aims at a spectroscopic study of hyperon resonances below the $\bar{K}N$ threshold via the (K^-, n) reaction on a deuteron target [9]. The primary goal of the experiment is to study the position and width of the $\Lambda(1405)$ resonance produced in the $\bar{K}N \to \pi\Sigma$ channel. For this reaction theoretical investigations were presented by Jido et al. in [10] and, with emphasis on the kinematical conditions of the DAFNE facility at Frascati, in [11]. Their calculation is performed in impulse approximation and considers for the reaction mechanism single ($\bar{K}N \to \pi\Sigma$) scattering but also the two-step process where the kaon first scatters off one of the nucleons and then undergoes the transition $\bar{K}N \to \pi\Sigma$ on the other nucleon. The required elementary $\bar{K}N \to \bar{K}N$ and $\bar{K}N \to \pi\Sigma$ amplitudes are taken from the Oset-Ramos model [12, 13] that utilizes the Weinberg-Tomozawa term as interaction potential. The model calculation of [10] yields results that are roughly in line with an old measurement of the $\pi^+\Sigma^-$ invariant mass spectrum for the reaction in question from 1977 [14]. Indeed the data exhibit a peak around $M_{\pi\Sigma} \approx 1425$ MeV, i.e. at roughly the energy where all modern $\bar{K}N$ interactions cited above predict a pole so that everything seemed to match perfectly. However, because some approximations are applied in the study of [10] this apparent success has to be taken with a grain of salt.

Our investigation intends to scrutinize the results of Ref. [10] in two aspects. First and most importantly, we want to avoid some of the approximations introduced in Ref. [10]. For example, we do not use factorization, i.e. we do not pull out the ($\bar{K}N \to \bar{K}N$ and $\bar{K}N \to \pi\Sigma$) amplitudes from the loop integral that occurs in the cal-

culation of the two-step process. Also, and more importantly, we treat the kinematics in the Green's function that appears in the loop integral properly. Specifically we make sure that the three-body unitarity cut for the intermediate $\bar{K}NN$ system occurs at the correct (physical) threshold. As we will see this has a decisive influence on the achieved results.

In addition, we also consider different models for the elementary $\bar{K}N$-$\pi\Sigma$ interaction. Practically all the interactions in the literature are fitted to the near-threshold cross sections for $\bar{K}N$ elastic and charge-exchange scattering and for the $\bar{K}N \to \pi\Lambda$ and $\bar{K}N \to \pi\Sigma$ transitions. As a consequence, the properties of these interactions in the $\bar{K}N$ threshold region are very similar, even down to the position of the (nominal) $\Lambda(1405)$ resonance. However, for energies further away from the threshold there is a significant model dependence. This is reflected, for example, in the large variation of the position of the lower pole, already mentioned above, see also [15]. Indeed there are phenomenological models that describe the data around the $\bar{K}N$ threshold with comparable quality, but do not even have a second pole [16]. It is interesting to see whether and how these model differences are reflected in the results for $K^- d \to \pi\Sigma N$. After all, the $\pi\Sigma$ invariant mass spectrum samples the properties of the $\bar{K}N$-$\pi\Sigma$ interaction down to the $\pi\Sigma$ threshold.

In the present study we utilize the Oset-Ramos interaction [12, 13] so that we can compare our results directly with other ones that can be already found in the literature [10]. The pole positions produced by this interaction in the isospin I=0 channel, which are associated with the $\Lambda(1405)$, are $1426 + i16$ MeV and $1390 + i66$ MeV [3], respectively. In addition we use a potential model that differs not only in the position of the lower pole from the Oset-Ramos interaction [12] but also conceptually. In particular, we resort to a meson-exchange potential of the $\bar{K}N$-$\pi\Sigma$ systems that was published by the Jülich group more than 20 years ago [17], i.e. long before the chiral unitary approach became popular. As can be seen in the original paper [17], the Jülich model describes the $\bar{K}N$ scattering data in the near-threshold region quite satisfactorily. Other threshold quantities are fairly well reproduced too, as shown in a recent paper [18]. Of importance for the present study is also that the Jülich model generates likewise two poles in the region of the $\Lambda(1405)$ resonance. One pole, the $\bar{K}N$ "bound state", is located fairly close to the $\bar{K}N$ threshold and to the physical real axis ($1436 + i26$ MeV) while the other one is close to the $\pi\Sigma$ threshold and has a significantly larger imaginary part ($1334 + i62$ MeV). In fact, this pole lies at the lower end of the "lower pole spectrum" mentioned above.

The paper is structured as follows: In the subsequent section we summarize shortly the salient features of the $\bar{K}N$ interaction of the Jülich group. In Sect. III we describe in detail the formalism that is employed in our calculation of the reaction $K^- d \to \pi\Sigma N$. The results of our calculation for the Oset-Ramos and the Jülich $\bar{K}N$ interactions are presented in Sect. IV. In particular, we discuss approximations applied in previous investigations and study their impact on the shape of the ΣN invariant mass spectrum. The manuscript closes with a summary.

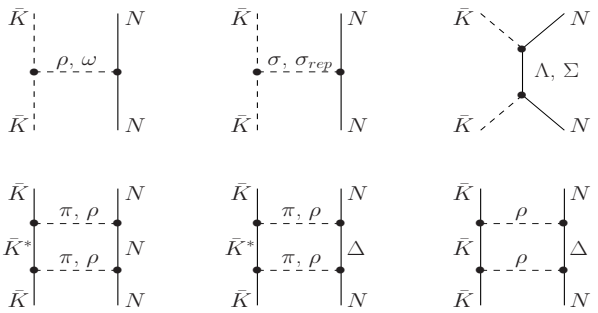

FIG. 1: Meson-exchange contributions included in the $\bar{K}N$ interaction.

II. THE JÜLICH $\bar{K}N$ MODEL

The Jülich meson-exchange model of the KN and $\bar{K}N$ interactions has been described in detail in the literature [21–24] and we refer the reader to those works. The interaction model was constructed along the lines of the (full) Bonn NN model [19] and its extension to the hyperon-nucleon (YN) system [20] ($Y = \Lambda,\ \Sigma$). Specifically, this means that one has used the same scheme (time-ordered perturbation theory), the same type of processes, and vertex parameters (coupling constants, cut-off masses of the vertex form-factors) fixed already by the study of these other reactions.

The diagrams considered for the $\bar{K}N$ interaction are shown in Fig. 1. Obviously the Jülich model contains not only single-meson exchanges, but also higher-order box diagrams involving $N\bar{K}^*$, $\Delta\bar{K}$ and $\Delta\bar{K}^*$ intermediate states. Most vertex parameters involving the nucleon and the $\Delta(1232)$ isobar are taken over from the (full) Bonn NN potential. The coupling constants at vertices involving strange baryons are fixed from the YN model (model B of Ref. [20]). Those quantities ($g_{N\Lambda K}$, $g_{N\Sigma K}$, g_{NY^*K}) have been related to the empirical $NN\pi$ coupling by the assumption of SU(6) symmetry, cf. Ref. [21, 22].

For the vertices involving mesons only, most coupling constants have been fixed by SU(3) relating them to the empirical $\rho \to 2\pi$ decay. An exception is the coupling constant $g_{KK\sigma}$, which has been adjusted to the KN data [21], for the following reason: The σ meson (with a mass of about 600 MeV) is not considered as a genuine particle but as a simple parametrization of correlated 2π-exchange processes in the scalar-isoscalar channel. Therefore, its coupling strength cannot be taken from symmetry relations. Concerning the ω-exchange the

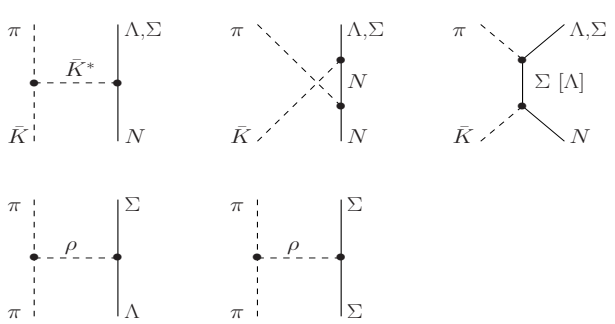

FIG. 2: Meson-exchange contributions included in the $\bar{K}N \to \pi\Lambda, \pi\Sigma$ transition potentials and in the $\pi\Lambda, \pi\Sigma \to \pi\Lambda, \pi\Sigma$ interactions.

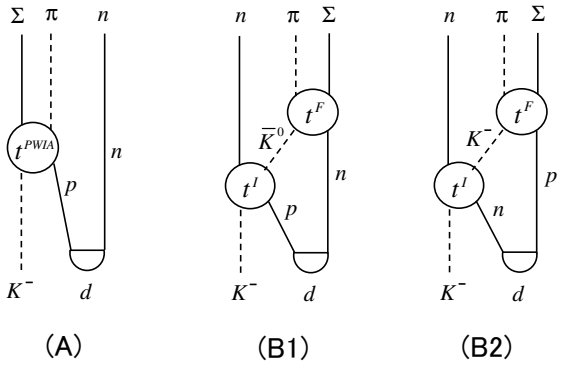

FIG. 3: Mechanisms included in our calculation of the reaction $K^-d \to \pi\Sigma n$. Plane-wave impulse-approximation (A); $\bar{K}^0 n \to \pi\Sigma$ (B1) and $K^-p \to \pi\Sigma$ (B2) rescattering, respectively.

coupling strengths for both $g_{NN\omega}$ and $g_{KK\omega}$ were kept at their SU(6) values. At the same time a phenomenological, very short-ranged contribution was added, denoted as σ_{rep}. This phenomenological piece has the same analytical form as σ-exchange, but an exchange mass of 1200 MeV and, most importantly, an opposite sign. Such a short-range contribution was required in order to obtain sufficient repulsion for a reasonable description of the S-wave KN phase shifts [21]. It was shown in Ref. [25] that this phenomenological piece can be explained dynamically, even on a quantitative level, by genuine quark-gluon exchange processes.

The contributions to the $\bar{K}N$ interaction in [22] are fixed from those of the KN model [21] via a G-parity transformation. The only exception is the phenomenological σ_{rep} whose strength is re-adjusted by a fit to $\bar{K}N$ data. Its contribution required there was found to be considerably reduced as compared to KN. Indeed, this is in line with the results of [25] because the quark-gluon exchange processes that generate most of the repulsion simulated by the σ_{rep} in case of KN are absent in the $\bar{K}N$ channel due to the different quark structure of the $\bar{K}$ meson.

Of course, in case of the $\bar{K}N$ system there are already open channels at the reaction threshold and the coupling to those channels ($\pi\Lambda$, $\pi\Sigma$) is taken into account explicitly. The diagrams considered for the $\bar{K}N \to \pi Y$ transitions and the $\pi Y \to \pi Y$ interactions are shown in Fig. 2. Also here SU(3) symmetry has been used for fixing the vertex parameters as far as possible.

With the $\bar{K}N$ potential and the $\bar{K}N \to \pi Y$ and the $\pi Y \to \pi Y$ transition interaction derived from the diagrams in Figs. 1 and 2, the reaction amplitude T is obtained by a solving a (coupled-channels) Lippmann-Schwinger type equation defined by time-ordered perturbation theory:

$$T_{\alpha\beta} = V_{\alpha\beta} + \sum_{\gamma} V_{\alpha\gamma} G_{0,\gamma} T_{\gamma\beta} \qquad (1)$$

with $\alpha, \beta, \gamma = \bar{K}N$, $\pi\Lambda$, $\pi\Sigma$.

III. FORMULATION OF $K^-D \to \pi\Sigma N$

In our study of the reaction $K^-d \to \pi\Sigma n$ we include the three diagrams shown in Fig. 3. Other 2-step processes in conjunction with process A in the form of a subsequent πn or Σn final-state interaction (FSI) are neglected. This is done because, as will be demonstrated later, the contribution from the process A to the cross section is a factor $10^2 \sim 10^3$ smaller than the one from process B2 in the considered region of incident K^- lab momenta around $p_{k^-} = 600$ MeV/c. The general expression of the cross section is given by

$$\begin{aligned} d\sigma \;=\; & \frac{1}{|\boldsymbol{v}_{K^-} - \boldsymbol{v}_d|} (2\pi)^4 \delta^4(p_n + p_\pi + p_\Sigma - p_{K^-} - p_d) \\ & \times \left| \langle \boldsymbol{p}_n | \langle \boldsymbol{p}_\pi | \langle \boldsymbol{p}_\Sigma | \, T \, | \boldsymbol{p}_{K^-} \rangle | \Phi_d \rangle \right|^2 \\ & \times \frac{d^3 p_n}{(2\pi)^3} \frac{d^3 p_\pi}{(2\pi)^3} \frac{d^3 p_\Sigma}{(2\pi)^3} \end{aligned} \qquad (2)$$

where the obvious dependence of the cross section on spin variables is omitted. The matrix element is given by

$$\begin{aligned} \langle \boldsymbol{p}_n | \quad & \langle \boldsymbol{p}_\pi | \langle \boldsymbol{p}_\Sigma | \, T \, | \boldsymbol{p}_{K^-} \rangle | \Phi_d \rangle \\ & = \sqrt{2} \; t^{PWIA}(\boldsymbol{p}_\pi \, \boldsymbol{p}_\Sigma \, , \, \boldsymbol{p}_{K^-} \tilde{\boldsymbol{p}}_1) \, \Phi_d(\tilde{\boldsymbol{p}}) \\ & + \sqrt{2} \int \frac{d^3 q_2}{(2\pi)^3} \, t^F(\boldsymbol{p}_\pi \, \boldsymbol{p}_\Sigma \, , \boldsymbol{q}_1 \boldsymbol{q}_2) \, G_0(\boldsymbol{q}_1 \boldsymbol{q}_2) \\ & \qquad \times t^I(\boldsymbol{q}_1 \, \boldsymbol{p}_n \, , \boldsymbol{p}_{K^-} \boldsymbol{p}_1) \, \Phi_d(\boldsymbol{p}) \; . \end{aligned} \qquad (3)$$

The first term on the right-hand side is the plane-wave impulse-approximation (PWIA) which is given by the contribution of diagram A, while the second term refers to diagram B, whose contribution will be discussed and

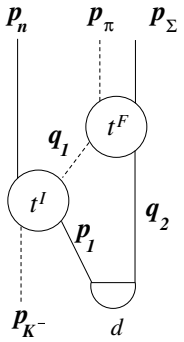

FIG. 4: Definition of the kinematical variables used in our calculation of the reaction $K^- d \to \pi\Sigma n$.

shown explicitly later on for the two possible intermediate particle states (B1 and B2). The factor $\sqrt{2}$ comes from the proper antisymmetrization. The quantities t^F and t^I denote the $\bar{K}N \to \pi\Sigma$ and $\bar{K}N \to \bar{K}N$ amplitudes, respectively. The various momentum variables which appear in the second term are depicted in Fig. 4. We work in the lab frame (deuteron rest frame), and then the momenta in Eq. (3) satisfy

$$\begin{aligned} \tilde{\boldsymbol{p}} &= \tilde{\boldsymbol{p}}_1 = -\boldsymbol{p}_n \,, \\ \boldsymbol{p} &= \boldsymbol{p}_1 = -\boldsymbol{q}_2 \,, \\ \boldsymbol{q}_1 &= \boldsymbol{p}_1 + \boldsymbol{p}_{K^-} - \boldsymbol{p}_n \,. \end{aligned} \tag{4}$$

The meson-baryon two-body energy E^I of the fully off-shell t-matrix t^I is given by

$$\begin{aligned} E^I &= E_{total} - \sqrt{\boldsymbol{q}_2^2 + m_N^2} \\ &= E_{K^-} + m_d - \sqrt{\boldsymbol{q}_2^2 + m_N^2} \,. \end{aligned} \tag{5}$$

Equations (2) and (3), presented here in a rather compact form, can be derived within a field theoretical approach in an appropriate manner (see, for example [26]). One only has to take care that the bound state deuteron in the initial state is incorporated, which should be described as a state in the Heisenberg representation (see also, for example [27]). Since we will use different interaction models for generating the t-matrices, derived in different frameworks, and a nonrelativistic deuteron wave function, those equations are not written in invariant form. Also notice that we assume that the intermediate $\bar{K}$ with momenta $\boldsymbol{q}_1$ propagates forward in time, so that the Green's function G_0 will be described only by the positive-frequency part. This is a quite reasonable treatment because we consider transitions to final states in the low-energy region around the $n\bar{K}N$ threshold.

Let us now derive the expression for the inclusive $d(K^-, n)\pi\Sigma$ cross section, where $\pi\Sigma$ indicates one of the charge states $\pi^+\Sigma^-$, $\pi^0\Sigma^0$, or $\pi^-\Sigma^+$. For evaluating the cross section it is convenient to take as integration variables the direction of the pion momentum $\boldsymbol{p}_\pi^{cm}$ in the center-of-mass (c.m.) frame of π and Σ. Thus, we first rewrite part of the phase space factor

$$\begin{aligned} & \delta^4 \ (p_n + p_\pi + p_\Sigma - p_{K^-} - p_d)\, d^3p_n\, d^3p_\pi\, d^3p_\Sigma \\ &= \ \delta(E_\pi^{cm} + E_\Sigma^{cm} - W_{\pi\Sigma})\, \delta^3(\boldsymbol{p}_\pi^{cm} + \boldsymbol{p}_\Sigma^{cm}) \\ &\quad \times \frac{E_\pi}{E_\pi^{cm}} \frac{E_\Sigma}{E_\Sigma^{cm}}\, d^3p_n\, d^3p_\pi^{cm}\, d^3p_\Sigma^{cm} \end{aligned} \tag{6}$$

where

$$W_{\pi\Sigma} = (E_{K^-} + m_d - E_n)^2 - |\boldsymbol{p}_{K^-} - \boldsymbol{p}_n|^2 \,. \tag{7}$$

Due to the 3-momentum δ-function, the integral over $\boldsymbol{p}_\Sigma^{cm}$ can be eliminated. Next, the quantity dp_π^{cm} is converted to $dM_{\pi\Sigma}$ by the following relation,

$$dp_\pi^{cm} = \frac{E_\pi^{cm}\, E_\Sigma^{cm}}{M_{\pi\Sigma}\, p_\pi^{cm}} dM_{\pi\Sigma} \,, \tag{8}$$

where $M_{\pi\Sigma} (= E_\pi^{cm} + E_\Sigma^{cm})$ is the invariant mass of the $\pi\Sigma$ system. We would like to integrate over the magnitude of the neutron momentum p_n, which is related to $W_{\pi\Sigma}$ by Eq. (7). Hence, the energy-conserving δ-function is substituted as

$$\begin{aligned} & \delta \quad (M_{\pi\Sigma} - W_{\pi\Sigma}) \\ &\quad = \frac{W_{\pi\Sigma}}{|(E_{K^-} + m_d)\, p_n/E_n - p_{K^-} \cos\theta_n|} \delta(\breve{p}_n - p_n), \end{aligned} \tag{9}$$

where θ_n is the polar angle of the neutron with regard to the K^- beam direction, and $\breve{p}_n$ satisfies

$$M_{\pi\Sigma} = (E_{K^-} + m_d - \breve{E}_n)^2 - |\boldsymbol{p}_{K^-} - \breve{\boldsymbol{p}}_n|^2 \,. \tag{10}$$

Performing the integral over p_n, we obtain the final expression of the inclusive cross section

$$\begin{aligned} & \frac{d\sigma}{dM_{\pi\Sigma}\, d\Omega_n} \\ &= \frac{1}{v_{K^-}(2\pi)^5} \frac{p_\pi^{cm}\, \breve{p}_n^2}{|(E_{K^-} + m_d)\, \breve{p}_n/\breve{E}_n - p_{K^-} \cos\theta_n|} \\ &\quad \times \int d\Omega_\pi^{cm}\, E_\pi E_\Sigma \left| \langle \breve{\boldsymbol{p}}_n | \langle \boldsymbol{p}_\pi | \langle \boldsymbol{p}_\Sigma |\, T\, | \boldsymbol{p}_{K^-} \rangle | \Phi_d \rangle \right|^2 . \end{aligned} \tag{11}$$

Now, let us discuss the second term of the right-hand side of Eq. (3) by introducing particle states explicitly. This term written out in detail amounts to

$$\sqrt{2}\ \langle n(1)|\, \langle \pi\, \Sigma(2)\, |\, t^F(2)\, G_0\, t^I(1)\, |\Phi_d\rangle |K^-\rangle \tag{12}$$

where the two baryons are numbered 1 and 2, and the argument 1 in the operator $t^I(1)$ indicates that it acts only on particle 1. The same holds for $t^F(2)$. The process corresponding to $t^F(1)\, G_0\, t^I(2)$ is absorbed into the factor $\sqrt{2}$. Applying the operator $t^I(1)$ on $|\Phi_d\rangle$ with the

isospin part of the deuteron written out explicitly yields

$$\begin{aligned}
&\langle n(1)|\, t^I(1)\,|\Phi_d\rangle|K^-\rangle \\
&= \langle n(1)|\, t^I(1)\,\frac{1}{\sqrt{2}}[|\,p(1)\rangle|\,n(2)\rangle - |\,n(1)\rangle|\,p(2)\rangle]\,|\,\phi_d\,\rangle|K^-\rangle \\
&= \frac{1}{\sqrt{2}}[\,|\,n(2)\rangle\langle n(1)|\, t^I(1)\,|p(1)K^-\rangle \\
&\qquad -|\,p(2)\rangle\langle n(1)|\, t^I(1)\,|n(1)K^-\rangle\,]\,|\,\phi_d\,\rangle\,. \qquad (13)
\end{aligned}$$

Inserting the complete set,

$$|\bar{K^0}n(2)\rangle\langle\bar{K^0}n(2)| + |K^-p(2)\rangle\langle K^-p(2)|,$$

between $t^F(2)G_0$ and $t^I(1)$ in Eq. (12) which is allowed by the total-charge conservation, we end up with

$$\begin{aligned}
\sqrt{2}\quad &\langle n(1)|\,\langle\pi\,\Sigma(2)\,|\,t^F(2)\,G_0\,t^I(1)\,|\Phi_d\rangle|K^-\rangle \\
&= \langle\pi\Sigma|\,t^F\,G_0\,|\bar{K^0}n\rangle\,\langle\bar{K^0}n|\,t^I\,|pK^-\rangle|\,\phi_d\,\rangle \\
&\quad -\langle\pi\Sigma|\,t^F\,G_0\,|K^-p\rangle\,\langle K^-p|\,t^I\,|nK^-\rangle|\,\phi_d\,\rangle, \qquad (14)
\end{aligned}$$

where the first term of the right-hand side corresponds to diagram B1 and the second term to diagram B2 in Fig 3. Obviously, there is an interference between these two terms.

Let us now come to the explicit expression of $G_0(\boldsymbol{q}_1\boldsymbol{q}_2)$ in Eq. (3). As already mentioned, the $\bar{K}$ with momenta $\boldsymbol{q}_1$ propagates forward in time and G_0 is described only by the positive-frequency part. Since we work in the lab frame, the Green's function is given by

$$\begin{aligned}
G_0(\boldsymbol{q}_1\boldsymbol{q}_2) &= \frac{1}{E_1 - E_1(q_1) + i\epsilon} \\
&= \frac{1}{E_\pi + E_\Sigma - E_2(q_2) - E_1(q_1) + i\epsilon}, \qquad (15)
\end{aligned}$$

where

$$\begin{aligned}
E_1 &\equiv E_{total} - E_n - E_2(q_2) \\
&= E_\pi + E_\Sigma - E_2(q_2), \qquad (16)
\end{aligned}$$

and

$$E_2(q_2) = \sqrt{\boldsymbol{q}_2^2 + m_N^2}\ , \quad E_1(q_1) = \sqrt{\boldsymbol{q}_1^2 + m_{\bar{K}}^2}\ . \qquad (17)$$

The total energy and the energies of the outgoing particles are indicated by E_{total} and by E_π, E_Σ, E_n, respectively. We can express the lab energies $E_\pi + E_\Sigma$ and $E_2(q_2) + E_1(q_1)$ in Eq. (15) by using the energies in the c.m. frame of the $\bar{K}N$ system. Then

$$G_0(q') = \frac{1}{\sqrt{\boldsymbol{P}^2 + M_{\pi\Sigma}^2} - \sqrt{\boldsymbol{P}^2 + W(q')^2} + i\epsilon}\,, \qquad (18)$$

where $\boldsymbol{P}$ is the $\bar{K}N$ total momentum, and $W(q')$ is defined by the momentum $\boldsymbol{q}'$ of the $\bar{K}$ in the c.m. frame:

$$\begin{aligned}
&\boldsymbol{P} = \boldsymbol{q}_1 + \boldsymbol{q}_2 = \boldsymbol{p}_\pi + \boldsymbol{p}_\Sigma \quad , \\
&W(q') = \sqrt{\boldsymbol{q}'^2 + m_{\bar{K}}^2} + \sqrt{\boldsymbol{q}'^2 + m_N^2} \quad . \qquad (19)
\end{aligned}$$

In order to expose the $n\bar{K}N$ three-body unitarity cut explicitly, we rewrite Eq. (18) as

$$\begin{aligned}
G_0(q') = \quad &\frac{1}{M_{\pi\Sigma} - W(q') + i\epsilon} \\
&\times \frac{\sqrt{\boldsymbol{P}^2 + M_{\pi\Sigma}^2} + \sqrt{\boldsymbol{P}^2 + W(q')^2}}{M_{\pi\Sigma} + W(q')}\,. \qquad (20)
\end{aligned}$$

In particular the singular part is given by

$$\frac{1}{M_{\pi\Sigma} - W(q') + i\epsilon} = \frac{1}{q_0^2 - q'^2 + i\epsilon}\, f(q_0,\, q')\,, \qquad (21)$$

where q_0 is defined by

$$W(q_0) = M_{\pi\Sigma}\,, \qquad (22)$$

and

$$\begin{aligned}
f(q_0,\, q')^{-1} = [E_1(q_0) \quad &+E_1(q')]^{-1} \\
&+[E_2(q_0) + E_2(q')]^{-1}\ . \qquad (23)
\end{aligned}$$

Consequently, one finds

$$\begin{aligned}
G_0(q') = \quad &\frac{1}{q_0^2 - q'^2 + i\epsilon}\, f(q_0,\, q') \\
&\times \frac{\sqrt{\boldsymbol{P}^2 + M_{\pi\Sigma}^2} + \sqrt{\boldsymbol{P}^2 + W(q')^2}}{M_{\pi\Sigma} + W(q')}\ . \qquad (24)
\end{aligned}$$

The c.m. momentum $\boldsymbol{q}'$ of the $\bar{K}$ is related to the lab momentum $\boldsymbol{q_2}$ of the nucleon by the relation [28]

$$\boldsymbol{q}' = \frac{\epsilon_2\boldsymbol{q}_1 - \epsilon_1\boldsymbol{q}_2}{\epsilon_1 + \epsilon_2} = -\boldsymbol{q}_2 + \frac{\epsilon_2}{\epsilon_1 + \epsilon_2}\boldsymbol{P}, \qquad (25)$$

where $\epsilon_i = (E_i + E_i^{cm})/2$, $(i = 1, 2)$. Thereby, in practice, we change the integral variable $\boldsymbol{q_2}$ in Eq. (3) to $\boldsymbol{q}'$ and then we can treat the $n\bar{K}N$ three-body cut in Eq. (24) precisely.

In the actual calculation the deuteron wave function of the Nijmegen soft-core potential Nijm93 [29] is employed. Test calculations performed with the wave function of the CD Bonn potential [30] led to practically identical results. Note that we used both the S and D wave components but the latter has no visible effect on the considered observables.

IV. RESULTS AND DISCUSSION

Inclusive cross sections for the reaction $d(K^-, n)\Sigma\pi$ are shown in Figs. 5 and 6 where the Jülich meson-exchange [17, 18] and the Oset-Ramos chiral interaction [12, 13] are used for generating the $\bar{K}N - \pi\Sigma$ amplitude, respectively. We fixed the K^- beam momentum to $p_{K^-} = 600$ MeV/c and the neutron angle to $\theta_n = 0^\circ$, considering the kinematics of the J-PARC experiment [9] where the neutron is planned to be detected at forward angle. Taking a

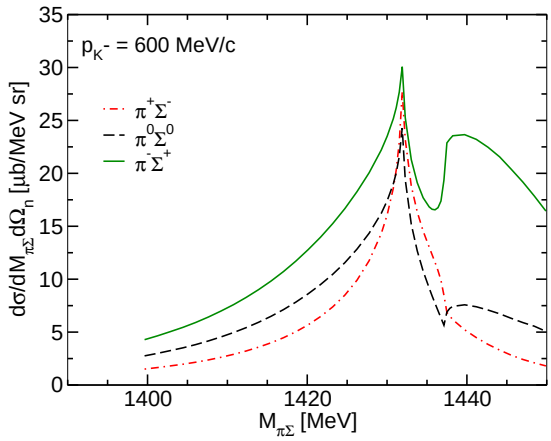

FIG. 5: $\pi\Sigma$ invariant mass spectrum for the reaction $K^- d \to \pi\Sigma n$ at the K^- beam momentum of 600 MeV/c and neutron angle $\theta_n = 0^\circ$. The $K^- N \to \pi\Sigma$ amplitudes of the Jülich model [17] are used.

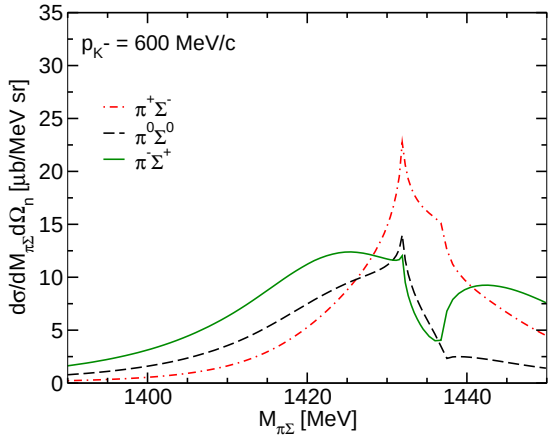

FIG. 6: $\pi\Sigma$ invariant mass spectrum for the reaction $K^- d \to \pi\Sigma n$ at the K^- beam momentum of 600 MeV/c and neutron angle $\theta_n = 0^\circ$. The $K^- N \to \pi\Sigma$ amplitudes of the Oset-Ramos model [13] are used.

glance at the figures, one immediately finds that no clear peaks are seen below the nK^-p threshold ($M_{\pi\Sigma} \simeq$1432 MeV) for both the Jülich and the Oset-Ramos potentials. Only for the $\pi^-\Sigma^+n$ final state of the latter interaction (Fig. 6) a fairly broad enhancement around $M_{\pi\Sigma} = 1425$ MeV is visible, however with a shape strongly deformed by the threshold. Obviously our results are in strong contradiction to the preceding work by Jido *et al.* [10] where the same kind of calculation, using the Oset-Ramos potential, shows clear peaks below the threshold for all of the three final states. In Ref. [10] lineshapes of the $\pi\Sigma$ invariant mass spectra integrated over neutron angles are presented but in Ref. [9] lineshapes limited to $\theta_n = 0^\circ$ are given by these authors, which exhibit similar peaks to the integrated ones. Since these peaks provide the basis of their argument with regard to the $\Lambda(1405)$ resonance position, first we want to clarify where this conspicuous difference comes from.

We start with examining the factorization approximation to the integral in Eq.(3), which is applied in Ref. [10]. Corresponding results are presented in Fig. 7. This approximation pulls the two amplitudes t^F and t^I out of the integral, fixing the momentum variables for these amplitudes to

$$\begin{aligned} \boldsymbol{p}_1 &= -\boldsymbol{q}_2 \approx 0\,, \\ \boldsymbol{q}_1 &\approx \boldsymbol{p}_{K^-} - \boldsymbol{p}_n \end{aligned} \tag{26}$$

which are the values that give the maximum of the deuteron wavefunction (see Eq. (4), and keep in mind that we work in the deuteron rest frame). Furthermore, the two-body energy E^I of the full off-shell t-matrix t^I is approximated by

$$\begin{aligned} E^I &= E_{total} - E_2(q_2) \\ &= E_{K^-} + m_d - E_2(q_2) \\ &\approx E_{K^-} + m_N \end{aligned} \tag{27}$$

(see Eq. (17) for the definition of $E_2(q_2)$). Then the second term of the right-hand side of Eq. (3) is expressed as

$$\begin{aligned} \sqrt{2} \int \frac{d^3q_2}{(2\pi)^3}\, & t^F(\boldsymbol{p}_\pi\, \boldsymbol{p}_\Sigma\,, \boldsymbol{q}_1 \boldsymbol{q}_2)\, G_0(\boldsymbol{q}_1 \boldsymbol{q}_2) \\ & \times t^I(\boldsymbol{q}_1\, \boldsymbol{p}_n\,, \boldsymbol{p}_{K^-} \boldsymbol{p}_1)\, \Phi_d(\boldsymbol{p}) \\ \approx \sqrt{2}\ & t^F_{app}\, t^I_{app} \\ & \times \int \frac{d^3q_2}{(2\pi)^3}\, G_0(\boldsymbol{q}_1 \boldsymbol{q}_2)\, \Phi_d(\boldsymbol{p})\,, \end{aligned} \tag{28}$$

where t^F_{app} and t^I_{app} are the pertinent amplitudes corresponding to the kinematics specified in Eqs. (26) and (27). In Fig. 7 we illustrate the effect of the factorization in the case of the final state $\pi^-\Sigma^+n$. One can see that the magnitude of the cross section is reduced by about 30%, but the lineshape remains practically unchanged.

Before moving to the more crucial approximation adopted in [10], we show individual contributions from the processes A, B1 and B2 (depicted in Fig. 3) where the factorization approximation is applied for B1 and B2, see Fig. 8. As already mentioned, the cross section for the process A is quite small. The large momentum of the outgoing neutron, which is directly emitted from the deuteron in the case of process A, leads to a tiny value of the deuteron wavefunction and suppresses the process (note that the momentum $\tilde{p}$ in Eqs. (3) and (4) is 3.9 fm^{-1} at the nK^-p threshold). As is seen in Fig. 8, the process B2 yields the main contribution. This is due to the fact that the amplitude $t^I(K^-n \to K^-n)$ that enters the process B2 is much larger than $t^I(K^-p \to \bar{K}^0 n)$

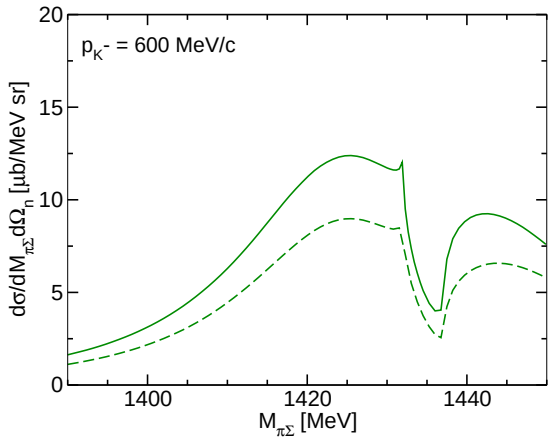

FIG. 7: $\pi^-\Sigma^+$ invariant mass spectrum for the reaction $K^-d \to \pi^-\Sigma^+ n$ at the K^- beam momentum of 600 MeV/c and neutron angle $\theta_n = 0^\circ$. The solid line is the correct result while the dashed line is obtained by factorizing the two-body amplitudes in the loop integral of the two-step process B. The $K^-N \to \pi\Sigma$ amplitudes of the Oset-Ramos model [13] are used.

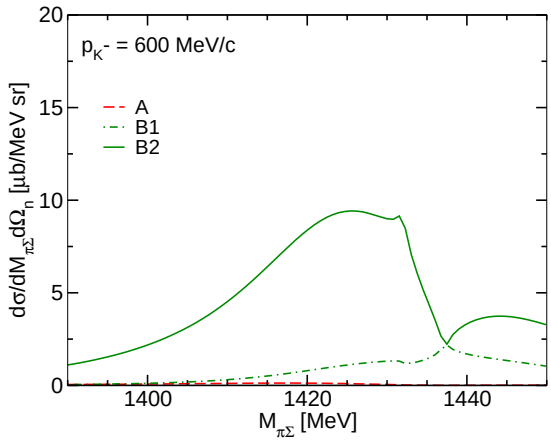

FIG. 8: $\pi^-\Sigma^+$ invariant mass spectrum for the reaction $K^-d \to \pi^-\Sigma^+ n$ at the K^- beam momentum of 600 MeV/c and neutron angle $\theta_n = 0^\circ$. The individual contributions from the reaction mechanisms A (dashed line), B1 (dash-dotted line), and B2 (solid line) are shown based on the factorization approximation. The $K^-N \to \pi\Sigma$ amplitudes of the Oset-Ramos model [13] are used.

in B1 at $p_{K^-} = 600$ MeV/c, something that was already pointed out in Ref. [10].

Now let us reveal why no clear peaks are seen in our results of the cross sections, in contrast to what was shown in Ref. [10]. In this reference the authors applied the same approximation as introduced to E^I in Eq. (27) also to the intermediate $\bar{K}$ energy E_1 in the propagator $G_0(\boldsymbol{q}_1\boldsymbol{q}_2)$ given in Eq. (16):

$$\begin{aligned} E_1 &= E_{total} - E_n - E_2(q_2) \\ &\approx E_{K^-} + m_N - E_n \end{aligned} \tag{29}$$

(see Eq. (14) in Ref. [10]). Then it follows that

$$\begin{aligned} G_0(\boldsymbol{q}_1\boldsymbol{q}_2) &= \frac{1}{E_{total} - E_n - E_2(q_2) - E_1(q_1) + i\epsilon} \\ &\approx \frac{1}{E_{K^-} + m_N - E_n - E_1(q_1) + i\epsilon} \ . \end{aligned} \tag{30}$$

This approximation has a serious impact on the lineshapes of the cross section as we will see. Comparing it with the expressions without the approximation, Eqs. (15), (18) and (24), one already suspects that it shifts the $n\bar{K}N$ three-body unitarity cut and the $n\bar{K}N$ threshold position.

In order to make the effect of this approximation more transparent we work within the factorization approximation (Eq. (28)) and we consider here the two ingredients that provide the dominant momentum dependence in the evaluation of the cross section separately, namely the $\bar{K}N \to \pi\Sigma$ amplitude t^F_{app} and the integral $\int d^3q_2\, G_0(\boldsymbol{q}_1\boldsymbol{q}_2)\, \Phi_d(\boldsymbol{p})$. We focus on the process B2 that yields the overall largest contribution. Results based on the assumption that the matrix element $\langle \boldsymbol{p}_n | \langle \boldsymbol{p}_\pi | \langle \boldsymbol{p}_\Sigma | \, T \, | \boldsymbol{p}_{K^-} \rangle | \Phi_d \rangle$ is given solely by the integral over the Green's function and the deuteron wave function are presented in Fig. 9 where the solid and dashed lines correspond to the cases without and with the approximation described by Eq. (30), respectively. One can see that the approximation shifts the nK^-p threshold to lower energies by an amount of 14 MeV as compared to its actual physical value. Furthermore, one realizes that the integral that enters Eq. (28) generates a characteristic behavior of the cross section at the threshold, in particular a rapid decrease below the threshold, which comes from the principal-value part of the integral over $G_0(\boldsymbol{q}_1\boldsymbol{q}_2)$.

In Fig. 10 we display results for the cross sections where the matrix element Eq. (28) is now assumed to be given by the amplitude t^F_{app} alone. The cross sections for the three charge states are displayed, each of which shows a clear peak around $M_{\pi\Sigma} = 1420$ MeV. As expected (and checked by us) those lineshapes agree pretty well with the *two-body* invariant mass distributions due to the $K^-p \to \pi\Sigma$ amplitudes. Finally, in Fig. 11, we plot the cross section based on the full matrix element of Eq. (28) but with the approximation of Eq. (30) for the Green's function. (Please note that in the employed factorization approximation this amounts practically to the product of the results shown in Figs. 9 and 10.) As already seen and discussed above, the nK^-p threshold is shifted to lower energies, specifically to $M_{\pi\Sigma} \simeq 1418$ MeV. As a consequence this artificial threshold position is then very close to the energy where the amplitude t^F_{app} has its peak so that this approximation generates a huge bump of the

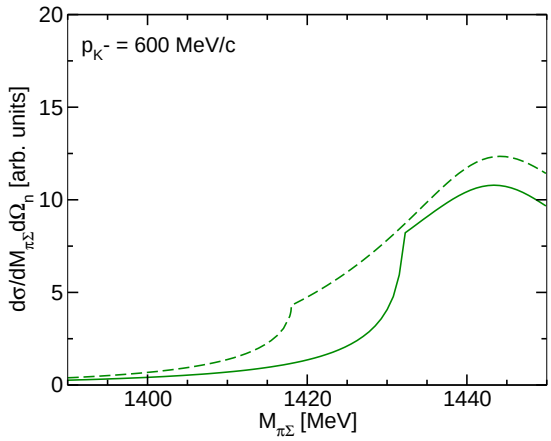

FIG. 9: $\pi\Sigma$ invariant mass spectrum for the reaction $K^- d \to \pi\Sigma n$ at the K^- beam momentum of 600 MeV/c and neutron angle $\theta_n = 0°$. Shown are results based on the integral over the Green's function alone, cf. Eq. (28), where either the correct expression Eq. (24) (solid line) or the approximation Eq. (30) (dashed line) are used.

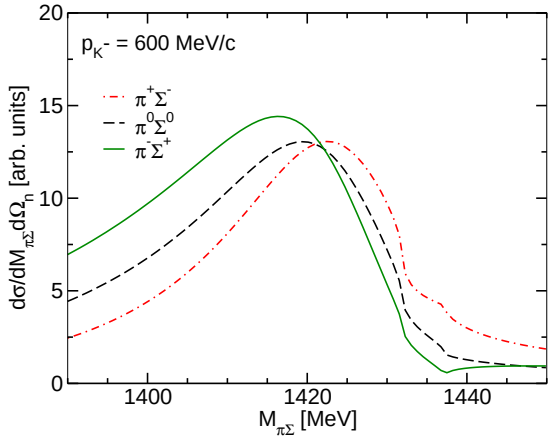

FIG. 10: $\pi\Sigma$ invariant mass spectrum for the reaction $K^- d \to \pi\Sigma n$ at the K^- beam momentum of 600 MeV/c and neutron angle $\theta_n = 0°$. The results are based on using only t^F_{app} in Eq. (28) and considering only the reaction mechanism B2. The $K^- N \to \pi\Sigma$ amplitudes of the Oset-Ramos model [13] is used.

cross section just at that energy. Please compare the result for the $\pi^-\Sigma^+ n$ final state in Fig. 11 with the solid line in Fig. 8 where the approximation of Eq. (30) is not made!

The above considerations strongly suggest that in a precise calculation where the three-body ($n\bar{K}N$) unitarity cut is implemented correctly the peaks which are present in the *two-body* amplitude t^F, due to the $\Lambda(1405)$,

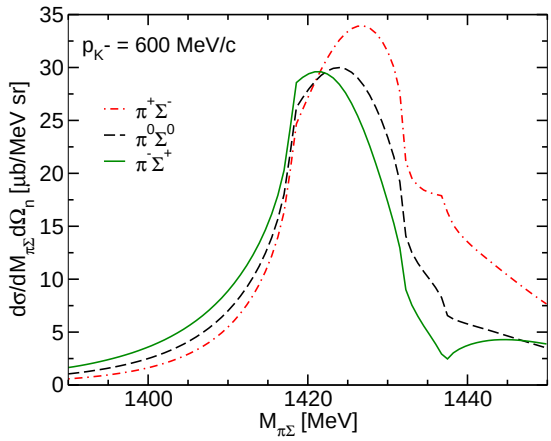

FIG. 11: $\pi\Sigma$ invariant mass spectrum for the reaction $K^- d \to \pi\Sigma n$ at the K^- beam momentum of 600 MeV/c and neutron angle $\theta_n = 0°$. The results are based on the approximation Eq. (30) considering only the reaction mechanism B2. The $K^- N \to \pi\Sigma$ amplitudes of the Oset-Ramos model [13] are used.

are suppressed by the threshold behavior of the Green's function $G_0(\boldsymbol{q}_1 \boldsymbol{q}_2)$, so that no clear peak (besides a threshold cusp) appears in the corresponding $\pi\Sigma$ invariant mass spectrum of the three-body final state. We believe that this explains the difference between our result and the one by Jido et al. [10]. In the latter the peak due to the $\Lambda(1405)$ in the three-body case is seen at practically the same invariant mass as in the two-body amplitude - because approximations are applied to the Green's function that shift the opening of the three-body cut to a lower invariant mass.

The success of the paper by Jido et al. in stimulating experimental efforts (and pertinent proposals) results not least from the fact that their calculation is roughly in line with data of an old measurement of the $\pi^+\Sigma^-$ invariant mass spectrum for the reaction in question from 1977 [14]. Those data suggest a peak around $M_{\pi\Sigma} \approx 1425$ MeV - and not at the nK^-p threshold! In our own calculation within a similar approach, but where now the nK^-p unitarity cut is implemented correctly, those data are no longer reproduced. However, we would like to emphasize that in a full calculation, where all rescattering processes are summed up to infinite order as it is the case in Faddeev-type approaches, it is certainly possible that the structure due to the $\Lambda(1405)$ could survive, after the characteristic behavior of $G_0(\boldsymbol{q}_1 \boldsymbol{q}_2)$ is smoothened out. Such a calculation would then not only have the opening of the nK^-p channel at the correct location, it would also fulfill exact three-body unitarity, which is not the case in our study (and also not in Ref. [10]) where only two-step processes are considered.

Since within our calculation based on two-step processes, the cross sections below the nK^-p threshold turn

out to be suppressed by the Green's function, we refrain from discussing the results below the threshold, i.e. in the $\Lambda(1405)$ resonance region, in detail. Rather we focus on the differences in the predictions for the $\pi\Sigma$ invariant mass spectra at $p_{K^-} = 600$ MeV/c based on the Jülich and the Oset-Ramos interactions, as seen in Figs. 5 and 6. To shed light on this difference let us compare the individual contributions from the processes B1 and B2 for the two interactions in question. This is done in Figs. 12 and 13, exemplary for the final states $\pi^0\Sigma^0 n$ and $\pi^-\Sigma^+ n$. As is clear from Fig. 12, the contributions from the process B2 predicted by those two interactions are very similar above the nK^-p threshold. On the other hand, the cross section for the process B1 by the Oset-Ramos interaction is much smaller than that of the Jülich potential and amounts to just about 40% as compared to the latter at the $n\bar{K}^0 n$ threshold, cf. Fig. 13. These two processes (B1 and B2) interfere and produce the differences seen between Figs. 5 and 6. We have confirmed that the difference due to B1 above comes from the difference of the amplitude $t^I(K^-p \to \bar{K}^0 n)$ in the relevant s wave. For example, the corresponding $K^-p \to \bar{K}^0 n$ (two-body) cross section at $p_{K^-} = 600$ MeV/c is 3.62 mb for the Jülich interaction while it is just 1.57 mb for the Oset-Ramos interaction. On the other hand, the K^-n elastic total cross sections at $p_{K^-} = 600$ MeV/c based on the amplitude $t^I(K^-n \to K^-n)$ that enters into the process B2 are similar for the two interactions: 13.8 mb for the Jülich and 13.5 mb for the Oset-Ramos interaction

TABLE I: Various $\bar{K}N$ s-wave cross sections in mb for $p_{K^-} \approx$ 600 MeV/c. Results are given for the Jülich [17] and Oset-Ramos (OR) [12] $\bar{K}N$ interactions and two partial wave analyses [31, 32].

channel	Jülich	OR	Alston [31]	Gopal [32]
$K^-p \to K^-p$	13.5	22.4	13.5	13.9
$K^-n \to K^-n$	13.8	13.5	6.9	7.5
$K^-p \to \bar{K}^0 n$	3.62	1.57	1.62	1.81

In table I we summarize the s-wave cross sections for various channels at $p_{K^-} = 600$ MeV/c and compare them with results of two partial wave analyses from the 1970s [31, 32]. Obviously the predictions of the Jülich model agree well with the s-wave K^-p scattering cross section deduced from empirical information but overshoot the other channels, while the Oset-Ramos interaction is only in line with phenomenology in case of the charge-exchange reaction. This may be not too surprising in view of the fact that both models were primarily designed to reproduce the $\bar{K}N$ data near threshold. On the other hand, it is obvious that for a future quantitative analysis of the reaction $K^-d \to \pi\Sigma n$, two-body amplitudes for $K^-n \to K^-n$ and $K^-p \to \bar{K}^0 n$ are required that are fully consistent with the available scattering data. Furthermore, one should not forget that at momenta around 600 MeV/c higher partial wave could already play a role,

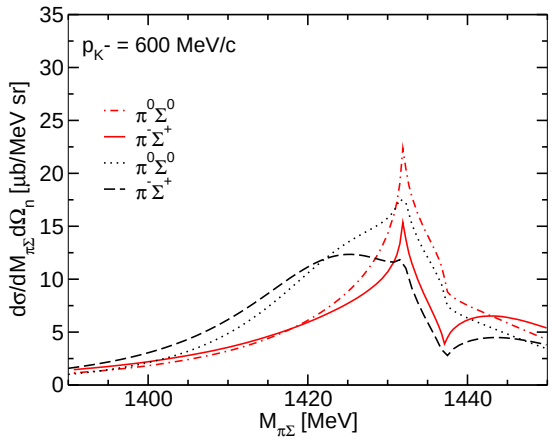

FIG. 12: $\pi\Sigma$ invariant mass spectrum for the reaction $K^-d \to \pi\Sigma n$ at the K^- beam momentum of 600 MeV/c and neutron angle $\theta_n = 0°$. Comparison of results based on the $K^-N \to \pi\Sigma$ amplitudes of the Jülich (dash-dotted and solid lines) [17] and the Oset-Ramos (dotted and dashed lines) [13] models. Only the reaction mechanism B2 is taken into account.

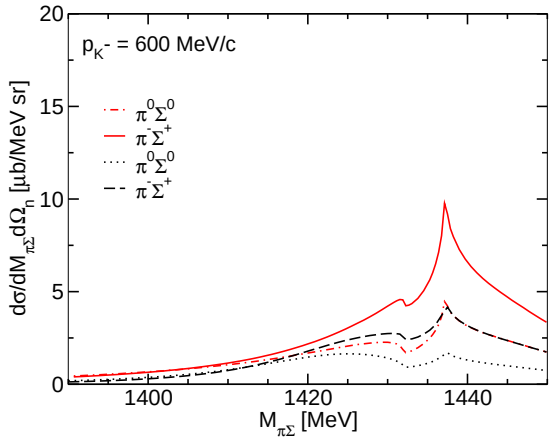

FIG. 13: $\pi\Sigma$ invariant mass spectrum for the reaction $K^-d \to \pi\Sigma n$ at the K^- beam momentum of 600 MeV/c and neutron angle $\theta_n = 0°$. Comparison of results based on the $K^-N \to \pi\Sigma$ amplitudes of the Jülich (dash-dotted and solid lines) [17] and the Oset-Ramos (dotted and dashed lines) [13] models. Only the reaction mechanism B1 is taken into account.

an issue which likewise has to be addressed in a quantitative analysis of upcoming experimental information.

V. SUMMARY

We investigated the reaction $K^-d \to \pi\Sigma N$ taking into account single scattering and the two-step process due to

$\bar{K}N \to \pi\Sigma$ rescattering. This reaction is considered as a promising candidate for exploring the properties of the $\Lambda(1405)$ resonance.

The main aim of our work was to examine the influence of some approximations applied in earlier studies of this reaction [10] on the results for the $\pi\Sigma$ invariant mass spectrum. In particular, in our study we did not use factorization, i.e. the $\bar{K}N \to \bar{K}N$ and $\bar{K}N \to \pi\Sigma$ amplitudes that enter into the calculation of the two-step process are not pulled out of the loop integral, and, more importantly, we treated the kinematics in the Green's function that appears in the loop integral properly. Specifically we made sure that the three-body unitarity cut for the intermediate $\bar{K}NN$ system occurs at the correct (physical) threshold. In addition we consider different models for the elementary $\bar{K}N$-$\pi\Sigma$ interaction.

We found that the factorization approximation leads to an overall reduction in the magnitude of the predicted invariant mass spectrum in the order of roughly 30%. However, the lineshape itself remains practically unchanged by this approximation. On the other hand, the approximation in the kinematics of the Green's function, also applied in the works of Jido et al. [10, 11], has a rather dramatic impact on the resulting lineshape. This approximation shifts the three-body cut due to the opening of the nK^-p threshold down by roughly 14 MeV from its physical value. It then coincides practically with the peak value of the elementary $\bar{K}N$-$\pi\Sigma$ amplitude that corresponds to the $\Lambda(1405)$ resonance and, consequently, the resulting lineshape exhibits a strong enhancement at a $\pi\Sigma$ invariant mass of around 1426 MeV. In contrast, a calculation where the nK^-p cut is taken into account precisely leads to a $\pi\Sigma$ invariant mass spectrum that has a pronounced peak around 1435 MeV, i.e. at the opening of the nK^-p channel. Indeed the peak is nothing else than a threshold effect (cusp). In that calculation the contribution of the rescattering process $\bar{K}N$-$\pi\Sigma$ around 1426 MeV, where this amplitude has its maximum, is already significantly suppressed by the deuteron wave function and the fall-off of the nK^-p Green's function. Thus, only a rather broad structure is visible in the spectrum for the case of the $\bar{K}N$-$\pi\Sigma$ generated from the Oset-Ramos interaction whereas for the Jülich $\bar{K}N$ model there is no direct sign at all of the $\Lambda(1405)$ resonance.

Interestingly, existing data on the $\pi^+\Sigma^-$ invariant mass spectrum from the reaction $K^-d \to \pi\Sigma N$ [14] seem to suggest a peak around $M_{\pi\Sigma} \approx 1425$ MeV - and not at the nK^-p threshold! Should that be confirmed in the planned measurements at J-PARC it would be certainly a sign for the inadequacy of the approach adopted so far in the pertinent investigations [10, 11]. And it would be a strong hint that one should rather rely on Faddeev-type approaches where all rescattering processes can be summed up to infinite order. Then the structure in the two-body amplitudes corresponding to the $\Lambda(1405)$ resonance can be generated within the three-body context in a consistent way. Moreover, exact three-body unitarity can be automatically fulfilled. Such a calculation is beyond the scope of the present investigation but we intend to address this issue in a future study.

Acknowledgments

We would like to thank A. Ramos for providing us with the code for the potential of Refs. [12, 13]. K.M. thanks Walter Glöckle for valuable discussions on the basic equations for the K^-d reaction.

[1] K. Nakamura et al. (Particle Data Group), J. Phys. G **37**, 075021 (2010).
[2] J.A. Oller and U.-G. Meißner, Phys. Lett. B **500**, 263 (2001).
[3] D. Jido, J. A. Oller, E. Oset, A. Ramos, and U.-G. Meißner, Nucl. Phys. A **725**, 181 (2003).
[4] C. Garcia-Recio, J. Nieves, E. Ruiz Arriola, and M. J. Vicente Vacas, Phys. Rev. D **67**, 076009 (2003).
[5] J.A. Oller, J. Prades, and M. Verbeni, Phys. Rev. Lett. **95**, 172502 (2005).
[6] B. Borasoy, R. Nißler, W. Weise, Eur. Phys. J. A **25**, 79 (2005).
[7] B. Borasoy, U.-G. Meißner, and R. Nißler, Phys. Rev. C **74**, 055201 (2006).
[8] M. Mai and U.-G. Meißner, arXiv:1202.2030 [nucl-th].
[9] S. Ajimura et al., http://j-parc.jp/NuclPart/pac_0907/pdf/Noumi.pdf
[10] D. Jido, E. Oset, and T. Sekihara, Eur. Phys. J. A **42**, 257 (2009).
[11] D. Jido, E. Oset, and T. Sekihara, Eur. Phys. J. A **47**, 42 (2011).
[12] E. Oset and A. Ramos, Nucl. Phys. A **635**, 99 (1998).
[13] E. Oset, A. Ramos and C. Bennhold, Phys. Lett. **B527**, 99 (2002).
[14] O. Braun et al., Nucl. Phys. B **129**, 1 (1977).
[15] Y. Ikeda, T. Hyodo, D. Jido, H. Kamano, T. Sato, and K. Yazaki, Prog. Theor. Phys. **125**, 1205 (2011).
[16] J. Révai and N.V. Shevchenko, Phys. Rev. C **79**, 035202 (2009).
[17] A. Müller-Groeling, K. Holinde, and J. Speth, Nucl. Phys. A **513**, 557 (1990).
[18] J. Haidenbauer, G. Krein, U.-G. Meißner and L. Tolos, Eur. Phys. J. A **47**, 18 (2011)
[19] R. Machleidt, K. Holinde, Ch. Elster, Phys. Rep. **149**, 1 (1987).
[20] B. Holzenkamp, K. Holinde, and J. Speth, Nucl. Phys. **A500**, 485 (1989).
[21] R. Büttgen, K. Holinde, A. Müller–Groeling, J. Speth, and P. Wyborny, Nucl. Phys. A **506**, 586 (1990).
[22] M. Hoffmann, J.W. Durso, K. Holinde, B.C. Pearce, and J. Speth, Nucl. Phys. A **593**, 341 (1995).
[23] R. Büttgen, K.Holinde, D. Lohse, A. Müller–Groeling, J.

Speth, and P. Wyborny, Z. Phys. C **46**, S167 (1990).
[24] P. Wyborny, M. Hoffmann, K.Holinde, and J. Speth, Phys. Rev. C **48**, 1376 (1993).
[25] D. Hadjimichef, J. Haidenbauer, and G. Krein, Phys. Rev. C **66**, 055214 (2002).
[26] J.D. Bjorken and S. Drell, *Relativistic Quantum Mechanics*, (McGraw-Hill, New York 1964).
[27] S. Weinberg, *The Quantum Theory of Fields I*, (Cambridge University Press, 1995).
[28] R. Fong and J. Sucher, J. Math. Phys. **5**, 456 (1964).
[29] V. G. J. Stoks, R. A. M. Klomp, C. P. F. Terheggen, and J. J. de Swart, Phys. Rev. C **49**, 2950 (1994).
[30] R. Machleidt, Phys. Rev. C **63**, 024001 (2001).
[31] M. Alston-Garnjost et al., Phys. Rev. D **18**, 182 (1978).
[32] G.P. Gopal et al., Nucl. Phys. B **119**, 362 (1977).